

# Video Salient Object Detection Using Spatiotemporal Deep Features

Trung-Nghia Le and Akihiro Sugimoto

**Abstract**—This paper presents a method for detecting salient objects in videos where temporal information in addition to spatial information is fully taken into account. Following recent reports on the advantage of deep features over conventional hand-crafted features, we propose the SpatioTemporal Deep (STD) feature that utilizes local and global contexts over frames. We also propose the SpatioTemporal Conditional Random Field (STCRF) to compute saliency from STD features. STCRF is our extension of CRF toward the temporal domain and formulates the relationship between neighboring regions both in a frame and over frames. STCRF leads to temporally consistent saliency maps over frames, contributing to the accurate detection of the boundaries of salient objects and the reduction of noise in detection. Our proposed method first segments an input video into multiple scales and then computes a saliency map at each scale level using STD features with STCRF. The final saliency map is computed by fusing saliency maps at different scale levels. Our intensive experiments using publicly available benchmark datasets confirm that the proposed method significantly outperforms state-of-the-art methods. We also applied our saliency computation to the video object segmentation task, showing that our method outperforms existing video object segmentation methods.

**Index Terms**—Video saliency, salient object detection, spatiotemporal deep feature, spatiotemporal CRF, video object segmentation.

## I. INTRODUCTION

Salient object detection from videos plays an important role as a pre-processing step in many computer vision applications such as video re-targeting[1], object detection[2], person re-identification[3], and visual tracking[4]. Conventional methods for salient object detection often segment each frame into regions and artificially combine low-level (bottom-up) features (e.g., intensity[5], color[5], edge orientation[6]) with heuristic (top-down) priors (e.g., center prior[7], boundary prior[5], objectness[6]) detected from the regions. Low-level features and priors used there are hand-crafted and are not sufficiently robust for challenging cases, especially when the salient object is presented in a low-contrast and cluttered background. Although machine learning based methods have been recently developed[8][9][10], they are primary for integrating different hand-crafted features[9][11] or fusing multiple saliency maps generated from various methods[8]. Accordingly, they usually fail to preserve object details when the salient object touches the image boundary or have the similar appearance with the background because hand-crafted features are unstable there.

Trung-Nghia Le is with the Department of Informatics, SOKENDAI (Graduate University for Advanced Studies), Tokyo, Japan.

Akihiro Sugimoto is with the National Institute of Informatics, Tokyo, Japan.

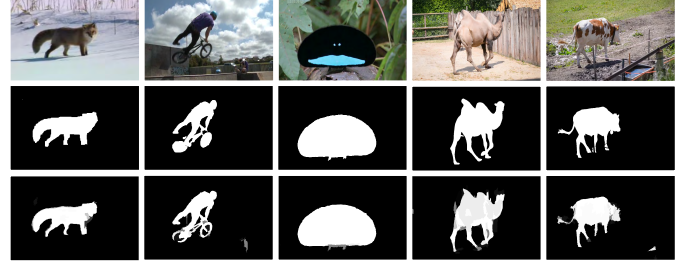


Fig. 1: Examples of results obtained by our proposed method. Top row images are original video frames, followed by the ground truth and corresponding saliency maps obtained using our method.

Recent advances in deep learning using Deep Neural Network (DNN) enable us to extract visual features, called deep features, directly from raw images/videos. They are more powerful for discrimination and, furthermore, more robust than hand-crafted features[12][13]. Indeed, saliency models for videos using deep features[14][15][16] have demonstrated superior results over existing works utilizing only hand-crafted features. They, however, extract deep features from each frame independently and employ frame-by-frame processing to compute saliency maps, resulting in not working well on dynamically moving objects. This is because temporal information over frames is not taken into account in computing either deep features or saliency maps.

Computed saliency maps do not always accurately reflect the shapes of salient objects in videos. To segment salient objects as accurately as possible while reducing noise, dense Conditional Random Field (CRF)[14][17], a powerful graphical model to globally capture the contextual information, has been applied to the computed saliency maps, which results in improving spatial coherence and contour localization. However, dense CRF is applied to each frame of a video separately, meaning that only spatial contextual information is considered. Again, temporal information over frames is not taken into account.

Motivated by the above observation, we propose a novel framework using spatiotemporal information as fully as possible for salient object detection in videos. We introduce the SpatioTemporal Deep (STD) feature that utilizes both local and global contexts over frames. Our STD feature consists of local and global features: The local feature aggregates over frames, deep features extracted from each frame using a region-based Convolutional Neural Network (CNN)[12], while the global feature is computed from a temporal-segment of

a video using a block-based CNN[13]. We also introduce the SpatioTemporal CRF (STCRF) totally based on STD features, in which the spatial relationship between regions in a frame as well as temporal consistency of regions over frames is formulated. Our proposed method first segments an input video into multi-scale levels and then at each scale level, extracts STD features and computes a saliency map. The method then fuses saliency maps at different scale levels into the final saliency map. Our extensive experiments on public benchmark datasets for video saliency confirm that our proposed method significantly outperforms the state-of-the-arts. Examples of saliency maps obtained by our method are shown in Fig.1. We also apply our method to video object segmentation and see that our method outperforms existing methods.

The rest of this paper is organized as follows. We briefly review and analyze related work in Section II. Then, we present in detail our proposed method in Section III. Intensive experiments are showed in Sections IV and V. In Section VI, we present an application of our proposed method to video object segmentation. Section VII presents conclusion and future work. We remark that a part of this work has been reported in [18].

## II. RELATED WORK

Here we briefly survey features used for salient object detection in videos, and saliency computation methods.

### A. Features for Salient Object Detection

Saliency computation methods for videos using hand-crafted features are mostly developed from traditional saliency models for still images by incorporating motion features to deal with moving objects[6][7][10][19]. Motion features commonly used there are optical flow[6][7][19] and trajectories of local features[10][20]. Other motion features such as gradient flow field[21] and temporal motion boundary[22] are also used: they are utilized to detect salient objects in videos. Xue et al.[23], on the other hand, sliced a video along  $X-T$  and  $Y-T$  planes to separate foreground moving objects from backgrounds. However, hand-crafted features have limitation in capturing the semantic concept of objects. Accordingly, these methods often fail when the salient object touches the image boundary or have the similar appearance with the background.

Several existing methods[14][24] for saliency computation using deep features, on the other hand, utilize superpixel segmentation to extract region-level deep features in different ways (e.g., feeding regions into a CNN individually to compute deep features[24] or pooling a pixel-level feature map into regions to obtain region-level deep features[14]). To exploit the context of a region in multiple scales, multi-scale deep features of the region are extracted by changing the window size[24]. Li et al.[24] fused multi-scale deep features of a region of interest to compute the saliency score for the region using a two-layer DNN. Hand-crafted features are also integrated into the deep features to improve accuracy for salient object detection[16]. Wang et al.[16] concatenated an

encoded low-level distance map and a high-level feature from CNN to enrich information included in the extracted feature. The region-level feature map and the pixel-level feature map are also integrated into the saliency model to enhance accuracy of detected object boundaries[14]. In end-to-end deep saliency models[15][25], pixel-based deep features are enhanced by their context information through recurrent CNNs.

Saliency models using deep features have demonstrated state-of-the-art performance in salient object detection and significantly outperformed existing works utilizing only hand-crafted features. However, temporal information over frames is not taken into account in deep features, resulting in these methods not working well on dynamically moving objects. Therefore, effectively utilizing spatial and temporal domains into powerful deep features for saliency computation is still opened to challenge.

### B. Saliency Computation Methods

The salient object detection approach using deep models [14][15][17][25][26] computes saliency scores directly from fully convolutional networks. In these deep models, recurrent layers[15][25] and skip connections[15][17] are utilized to boost up the contextual information of deep feature maps to enhance accuracy of saliency computation. However, these methods focus on frame-by-frame processing without considering any temporal information in videos. Thus, they do not work well on dynamically moving objects in videos. In addition, they still do not detect boundaries of salient objects accurately. The refinement as a post-processing is usually required for them to improve accuracy of detected object boundaries.

Spatial CRF has the capability of relating neighboring regions to capture the global context and has been commonly used for the refinement in semantic segmentation[27] and the saliency computation[14][17]. The dense CRF[28] is used as a post-processing to refine the label map generated from CNNs to improve the performance of semantic segmentation[27]. Shimoda et al.[27] developed a weakly supervised semantic segmentation method using a dense CRF to refine results from distinct class saliency maps. The Dense CRF is incorporated into the saliency map computed from the CNN to improve spatial coherence and contour localization[14][17]. Though spatial information is successfully utilized using CRFs in these methods, how to deal with temporal information is left to be considered, which is crucial for videos.

Dynamic CRF (DCRF)[29] is extended from the spatial CRF toward to the spatiotemporal domain to exploit both spatial and temporal information in videos. DCRF is constructed from consecutive video frames, where each pixel connects to its neighboring pixels in both space (i.e., the same frame) and time (i.e., the next frame and the previous frame). DCRF has been used to enhance both spatial accuracy and temporal coherence for object segmentation[29][30][31] and saliency computation[10] in videos. Yi et al.[31] proposed a framework using DCRF to improve fence segmentation in videos. Wang et al.[29][30] applied DCRF to object segmentation and moving shadow segmentation in indoor video scenes.

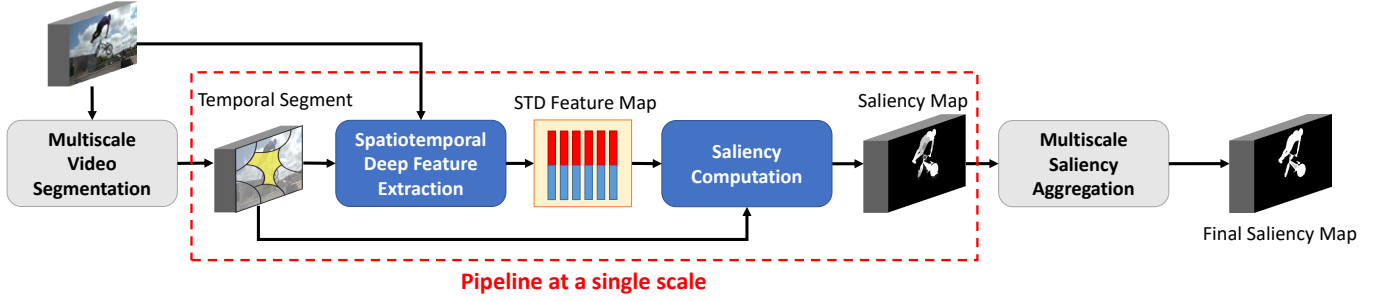


Fig. 2: Pipeline of the proposed method.

SIFT flow features were incorporated into DCRF to detect salient objects from videos[10]. However, DCRF is the pixel-level dense graph; thus it is usually constructed using only two successive frames due to large memory consumption. In addition, since the energy function of DCRF is totally based on the combination of classical hand-crafted features such as color and optical flow, DCRF lacks exploiting spatial and temporal information semantically. Our proposed STCRF differs from DCRF in that STCRF is defined over regions using STD features only so that it is capable of dealing with more successive frames and exploiting spatial and temporal information more semantically with less computational cost.

Differently from the existing methods, our proposed method utilizes spatiotemporal information as much as possible in both extracting deep features and computing saliency maps. Our proposed saliency computation using STD features with STCRF produces accurate saliency maps in both spatial and temporal domains. In particular, boundaries of salient objects are accurately detected with reducing noise.

### III. PROPOSED METHOD

#### A. Overview

Our goal is to compute the saliency map to accurately segment salient objects in every frame from an input video with keeping in mind that temporal information is as fully used as possible. Figure 2 illustrates the pipeline of our proposed method.

We segment an input video at multiple scales and compute a saliency map at each scale at each frame, and then aggregate all saliency maps at different scales at each frame into the final saliency map. This follows our intuition that objects in a video contain various salient scale patterns and an object at a coarser scale may be composed of multiple parts at a finer scale. In this work, we employ the video segmentation method[32] at four scale levels. After segmentation process, we obtain multiple scale temporal superpixels. At each scale, corresponding superpixels are connected across frames. We also remark that each segmentation level has a different number of superpixels, which are defined as non-overlapping regions.

The final saliency map is computed by taking the average value of saliency maps over different scales. In the following subsections, we explain how to compute a saliency map at a

scale. We remark that a saliency map in this section indicates the saliency map at a scale unless explicitly stated with "final."

#### B. Spatiotemporal Deep Feature Extraction

Our proposed STD feature is the concatenation of local and global features. The local feature is extracted using a region-based CNN followed by aggregation over frames, while the global feature is computed using a block-based CNN whose input is a temporal segment of the video. The STD feature extraction is illustrated in Fig.3.

1) *Local feature extraction:* A segmented region, namely, a superpixel, at each frame is fed into a region-based CNN to extract its region-based feature. As our region-based CNN, we use the publicly available R-CNN model[12] that was pre-trained on the ImageNet ILSVRC-2013 challenge dataset[33]. We note that we execute no fine-tuning in extracting region-based features.

The region-based feature contains the local context of the region but does not contain temporal information because it is computed frame-wisely. In order to incorporate temporal information, we aggregate region-based features over frames, resulting in the consistent local feature over frames. Just uniformly averaging region-based features over frames is not wise because pixel fluctuation occurring over time due to the lossy compression, degrades accuracy of corresponding regions over frames. This degradation becomes larger with respect to the time distance of frames. We thus linearly combine region-based features at neighboring frames, similarly to [6], using weights modeled by the Gaussian distribution centered at the frame to compute its local feature. With these weights, region-based features at frames having larger distances to a frame of interest, less contribute to the local feature of the frame: the local feature  $F_L(i, t)$  of a region  $i$  at frame  $t$  is extracted by

$$F_L(i, t) = \frac{1}{\Psi} \sum_{t'=t-k/2}^{t+k/2} \mathcal{G}(t'|t, \sigma^2) f(i, t'),$$

where  $f(i, t')$  is the region-based feature of region  $i$  at frame  $t'$ , and  $k = 16$  denotes the number of participating frames in the operation.  $\mathcal{G}(t'|t, \sigma^2)$  is a Gaussian distribution with mean  $t$  and standard deviation  $\sigma = 2$  expressing distribution of temporal weights.  $\Psi$  is the normalization factor.

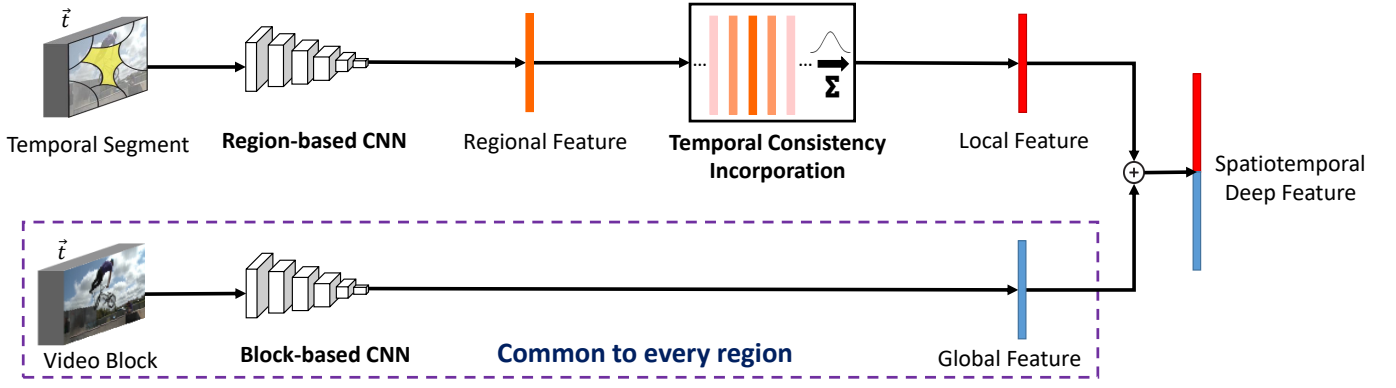


Fig. 3: Spatiotemporal Deep Feature Extraction.

2) *Global feature extraction*: To compute global features, we feed a temporal segment (sequential frames) of a video into a block-based CNN. The global feature obtained in this way takes its temporal consistency into account in its nature. As our block-based CNN, we employ the C3D model[13] pre-trained on the Sports-1M dataset[34], which is known to be effective for extracting spatiotemporal features for action recognition. As temporal segments, frame  $t$  is expanded into both directions in the temporal domain to obtain a 16-frame block as suggested by [13]. For each input block, we feed it into the pre-trained C3D model only once and assign the extracted global feature  $F_G(t)$  identically to all the regions in the block. This distributes the global context to each region and, at the same time, reduces the computational cost.

Finally, for each region of each frame, we concatenate its local and global features to obtain the STD feature  $F(i, t)$  of the region  $i$  at frame  $t$  whose dimension is  $4096 \times 2$ :  $F(i, t) = F_L(i, t) \oplus F_G(t)$ .

### C. Saliency Computation using SpatioTemporal CRF

CRF is used to enhance accuracy (particularly in object boundaries) of the saliency map while reducing noise because CRF captures the spatial relationship between regions in a frame. We extend CRF toward the temporal domain to have the ability to capture temporal consistency of regions over frames as well. We call our extended CRF, SpatioTemporal CRF (STCRF in short).

1) *STCRF Graph Construction*: For a segmented temporal region in a block (temporal-segment) of the video, i.e., temporal superpixels, at a scale, we construct a STCRF graph. Each vertex of the graph represents a region in the block, and each edge represents the neighboring relationship between regions in space or in time. Considering all the neighboring relationships, however, leads to a dense graph especially when the video volume is large, and the constructed graph becomes practically useless in the sense of memory consumption and processing time in the inference. We therefore restrict such edges only that represents the adjacency relationship (cf. Fig. 4). Furthermore, we partition the video into chunks of consecutive blocks so that inference in each block is performed separately.

In the experiments, an input video is decomposed into overlapping blocks with a fixed size where the overlapping rate is 50%. We note that each block length is equal to 16 frames (see Section V-B4). The saliency score of a region is refined by uniformly averaging saliency scores of the region over all the blocks having the region. This reduces processing time while keeping accuracy.

2) *Energy Function for STCRF*: We define the energy function of the STCRF so that probabilistic inference is realized by minimizing the function. The energy function  $E$  has a block (temporal segment)  $\mathbf{x}$  as its input.  $E$  is defined by the unary and the binary terms with labels representing foreground/background  $\mathbf{l} = \{l_i \in \{0, 1\} | i \in \mathcal{V}\}$  where  $l_i$  is the label for region  $i$  and  $\mathcal{V}$  is the set of vertices, i.e., regions in block  $\mathbf{x}$ :

$$E(\mathbf{l}, \mathbf{x}; \boldsymbol{\theta}) = \sum_{i \in \mathcal{V}} \psi_u(l_i; \theta_u) + \sum_{(i,j) \in \mathcal{E}} \psi_b(l_i, l_j; \theta_b),$$

where  $\psi_u$  and  $\psi_b$  are the unary and binary potentials given below.  $\mathcal{E}$  is the set of edges of the STCRF graph.  $\boldsymbol{\theta} = (\theta_u, \theta_b)$  is the model parameter.

#### Unary potential:

The unary potential for region  $i$  is defined using the label of the region:

$$\psi_u(l_i; \theta_u) = \theta_u \omega(F(i, t_i)),$$

where  $t_i$  is the frame in which region  $i$  exists, and  $\omega$  is a function predicting the foregroundness of a given region.

To compute  $\omega$ , i.e., the probability of foregroundness for each region, we employ the DNN proposed by Wang et al. [35] with our modifications. Our used network, called Foreground - Deep Neural Network (F-DNN in short), consists of 7 fully connected layers. Each layer executes a linear transformation followed by the Rectified Linear Unite (ReLU) [36]. Dropout operations are applied after ReLU layers during the training process for speed-up and for avoiding over-fitting. In our network, the output channels of the first three fully connected layers are 2048, and those of the next three layers are 1024. The last fully connected layer has 2 output channels. Denoting a fully connected layer, a ReLU layer, and a dropout layer by  $fc\#$ ,  $relu\#$ , and  $dropout\#$ , respectively, the structure of the network can be described as follows:  $fc1(2048) - relu1 -$

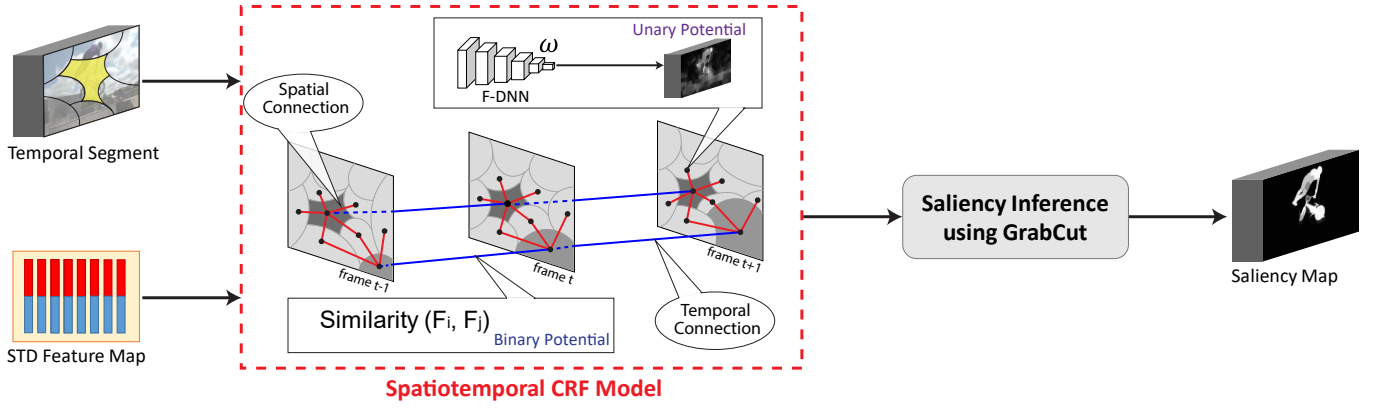


Fig. 4: Saliency Computation based on Graphical Model

dropout1 - fc2(2048) - relu2 - dropout2 - fc3(2048) - relu3 - dropout3 - fc4(1024) - relu4 - dropout4 - fc5(1024) - relu5 - dropout5 - fc6(1024) - relu6 - fc7(2).

#### Binary potential:

The binary potential provides the deep feature based smoothing-term that encourages to assign similar labels to regions with similar deep features. Depending on spatial adjacency or temporal adjacency, the potential is differently formulated with further separation of  $\theta_b$  into  $\theta_{bs}$  and  $\theta_{bt}$ :

$$\psi_b(l_i, l_j; \theta_b) = \begin{cases} \theta_{bs} \Phi_{bs}(l_i, l_j) & (i, j) \in \mathcal{E}_s \\ \theta_{bt} \Phi_{bt}(l_i, l_j) & (i, j) \in \mathcal{E}_t \end{cases},$$

where  $\mathcal{E}_s$  and  $\mathcal{E}_t$  denotes the set of edges representing spatial adjacency and that representing temporal adjacency. Namely,  $\mathcal{E} = \mathcal{E}_s \cup \mathcal{E}_t$  and  $\mathcal{E}_s \cap \mathcal{E}_t = \emptyset$ .

$\Phi_{bs}$  and  $\Phi_{bt}$  are spatial smoothness and temporal smoothness between two regions:

$$\begin{aligned} \Phi_{bs}(l_i, l_j) &= (1 - \delta_{l_i l_j}) D(i, j)^{-1} \exp\left(-\beta_s \|F(i, t_i) - F(j, t_j)\|^2\right), \\ \Phi_{bt}(l_i, l_j) &= (1 - \delta_{l_i l_j}) \phi(i, j) \exp\left(-\beta_t \|F(i, t_i) - F(j, t_j)\|^2\right), \end{aligned}$$

where  $\delta$  is the Kronecker delta and  $D(i, j)$  is the Euclidean distance of the centers of two regions  $i$  and  $j$ .  $\phi$  is the ratio of the area corresponded by the optical flow inside the two temporally different regions[37].  $F(i, t_i)$  is the STD feature of region  $i$  (which exists in frame  $t_i$ ). The parameters  $\beta_s$  and  $\beta_t$  are chosen similarly to [38] to ensure the exponential term switches appropriately between high and low contrasts:

$$\begin{aligned} \beta_s &= \frac{1}{2} \left( \sum_{(i, j) \in \mathcal{E}_s} \|F(i, t_i) - F(j, t_j)\|^2 \right)^{-1}, \\ \beta_t &= \frac{1}{2} \left( \sum_{(i, j) \in \mathcal{E}_t} \|F(i, t_i) - F(j, t_j)\|^2 \right)^{-1}. \end{aligned}$$

We remark that to compute  $\phi$ , we first count the area transformed from a temporal superpixel (region) at a frame to its corresponding region at the next frame via optical flow and vice versa, and then takes the average of ratios of the areas

against the regions. In the temporal domain, this weight is better than the Euclidean distance because it is independent of the speed of the motion[37]. In this work, we employ the deep flow method[39] to transfer pixels in the temporal superpixel.

3) *Saliency Inference*: Saliency scores for regions are obtained in terms of labels by minimizing the energy function:

$$\hat{l} = \arg \min_l E(l, x; \theta),$$

We minimize  $E$  using the GrabCut[38], which shows the effectiveness in CRF-based energy minimization[40], and is popularly used for object segmentation[41][42]. The minimization is executed as the iterative expectation-maximization[43] scheme until convergence. In each iteration, the Graph Cut algorithm[44] is used to solve the "Min-Cut/Max-Flow" problem[45] of the graph, resulting in a new label for each vertex (region). The updated labels are used for the next iteration.

## IV. EXPERIMENTAL SETTINGS

### A. Benchmark Datasets

We evaluated the performance of our method on three public benchmark datasets: 10-Clips dataset[46], SegTrack2 dataset[47], and DAVIS dataset[48].

**The 10-Clips dataset**[46] has ten video sequences in each of which a single salient object is present. Each sequence in the dataset has the spatial resolution of  $352 \times 288$  and consists of about 75 frames.

**The SegTrack2 dataset**[47] contains 14 video sequences and is originally designed for video object segmentation. A half of videos in this dataset have multiple salient objects. This dataset is challenging in that it has background-foreground color similarity, fast motion, and complex shape deformation. Sequences in the dataset consist of about 76 frames with various resolutions.

**The DAVIS dataset**[48] consists of 50 high quality  $854 \times 480$  spatial resolution and Full HD 1080p video sequences with about 70 frames per video, each of which has one single salient object or two spatially connected objects either with low contrast or overlapping with image boundary. This is also a challenging dataset because of frequent occurrences of occlusions, motion blur, and appearance changes. In this work,



we used only  $854 \times 480$  resolution video sequences whose number is 50.

All the datasets contain manually annotated pixel-wise ground-truth for every frame.

### B. Evaluation Criteria

We evaluated the performance using Precision-Recall Curve (PRC), F-measure [49], and Mean Absolute Error (MAE).

The first two evaluation metrics are computed based on the overlapping area between obtained results and provided ground-truth. Using a fixed threshold between 0 and 255, pairs of (*Precision*, *Recall*) scores are computed and then combined to form a PRC. F-measure is a balanced measurement between *Precision* and *Recall* as follows:

$$F_\beta = \frac{(1 + \beta^2) \text{Precision} \times \text{Recall}}{\beta^2 \times \text{Precision} + \text{Recall}}.$$

We remark that we set  $\beta^2 = 0.3$  for F-measure, as suggested by [49] so that precision is more considered.

For a given threshold, we binarize the saliency map to compute *Precision* and *Recall* at each frame in a video and then take the average over frames in the video. After that, the mean of the averages over videos in a dataset is computed. F-measure is computed from the final precision and recall. When binarizing results for the comparison with the ground truth, we used F-Adap[50], an adaptive threshold  $\theta = \mu + \eta$  where  $\mu$  and  $\eta$  are the mean value and the standard deviation of the saliency scores of the obtained map, and F-Max[51], which describes the maximum of F-measure scores for different thresholds from 0 to 255.

MAE, on the other hand, is the average over the frame of pixel-wise absolute differences between the ground truth  $GT$  and obtained saliency map  $SM$ :

$$\text{MAE} = \frac{1}{W \cdot H} \sum_{x=1}^W \sum_{y=1}^H \|SM(x, y) - GT(x, y)\|,$$

where  $W$  and  $H$  are the width and the height of the video frame. We note that MAE is also computed from the mean average value of the dataset in the same way as F-measure.

### C. Implementation details

We implemented our method using MATLAB and C/C++, using Caffe[52] for the DNN implementation.

To segment a video, we set the number of initial superpixels at each frame as  $\{100, 200, 300, 400\}$  at four scale levels. For parameters in STCRF, we empirically set  $\theta = (\theta_u, \theta_{bs}, \theta_{bt}) = (50, 0.05, 1000)$ . All these parameters are fixed throughout experiments.

All experiments were conducted on a PC with a Core i7 3.6GHz processor, 32GB of RAM, and GTX 1080 GPU. For a video with the resolution of  $352 \times 288$  and with the length of 100 frames, it took 431 seconds (238 seconds for STD feature extraction, 193 seconds for saliency computation). This excludes time for video segmentation. Note that video segmentation is usually slow.

TABLE I: Number of videos used in our experiments.

Dataset	10-Clips[46]	SegTrack2[47]	DAVIS[48]	Total
Training	6	8	30	44
Testing	4	6	20	30

TABLE II: Compared state-of-the-art methods and classification.

Target	Hand-crafted feature	Deep feature
Video	LC[20], LD[10], LGFOGR[21], LRSD[23], RST[6], SAG[22], SEG[19], STS[7]	None
Image	None	DCL[14], DHS[15], DS[26], DSS[17], ELD[16], MDF[24], RFCN[25]

### D. Training F-DNN for foregroundness prediction

In training our F-DNN (see Section III-C2), we took an approach that we use all three datasets together rather than training our F-DNN for each dataset. This is because each dataset is too small to train a reliable model. Our approach also enables the trained model not to over-fit to a specific dataset.

From each video dataset except for the DAVIS dataset, we chose randomly 60% the number of videos and mixed them into a larger dataset for training while the remaining videos were used for testing each dataset (cf. Table I). For the DAVIS dataset, we used the training set and the testing set as in the DAVIS Benchmark[48]<sup>1</sup>. We thus used 44 videos for training.

The model was fine-tuned from the network proposed in [35] using randomly initialized weights for new layers. We trained the network for 300k iterations, using the Stochastic Gradient Descent (SGD) optimization[53] with a moment  $\beta = 0.9$  and a weight decay of 0.005. The size of each mini-batch is set 500. A base learning rate was initially set to 0.001 and divided by 10 at every 50k iterations.

## V. EXPERIMENTAL RESULTS

### A. Comparison with the State-of-the-Arts

We compared the performance of our method (denoted by STCRF) with several state-of-the-art methods for salient object detection such as LC[20], LD[10], LGFOGR[21], LRSD[23], RST[6], SAG[22], SEG[19], STS[7], DCL[14], DHS[15], DS[26], DSS[17], ELD[16], MDF[24], and RFCN[25]. Compared methods are classified in Table II. We remark that we run their original codes provided by the authors with the recommended parameter settings for obtaining results. We also note that we frame-wisely applied to videos, the methods developed for the still image.

Figure 5 shows examples of obtained results. Qualitative evaluation confirms that our method produces the best results on each dataset. Our method can handle complex foreground and background with different details, giving accurate and uniform saliency assignment. In particular, object boundaries are clearly kept with less noise, compared with the other methods.

<sup>1</sup><http://davischallenge.org/browse.html>

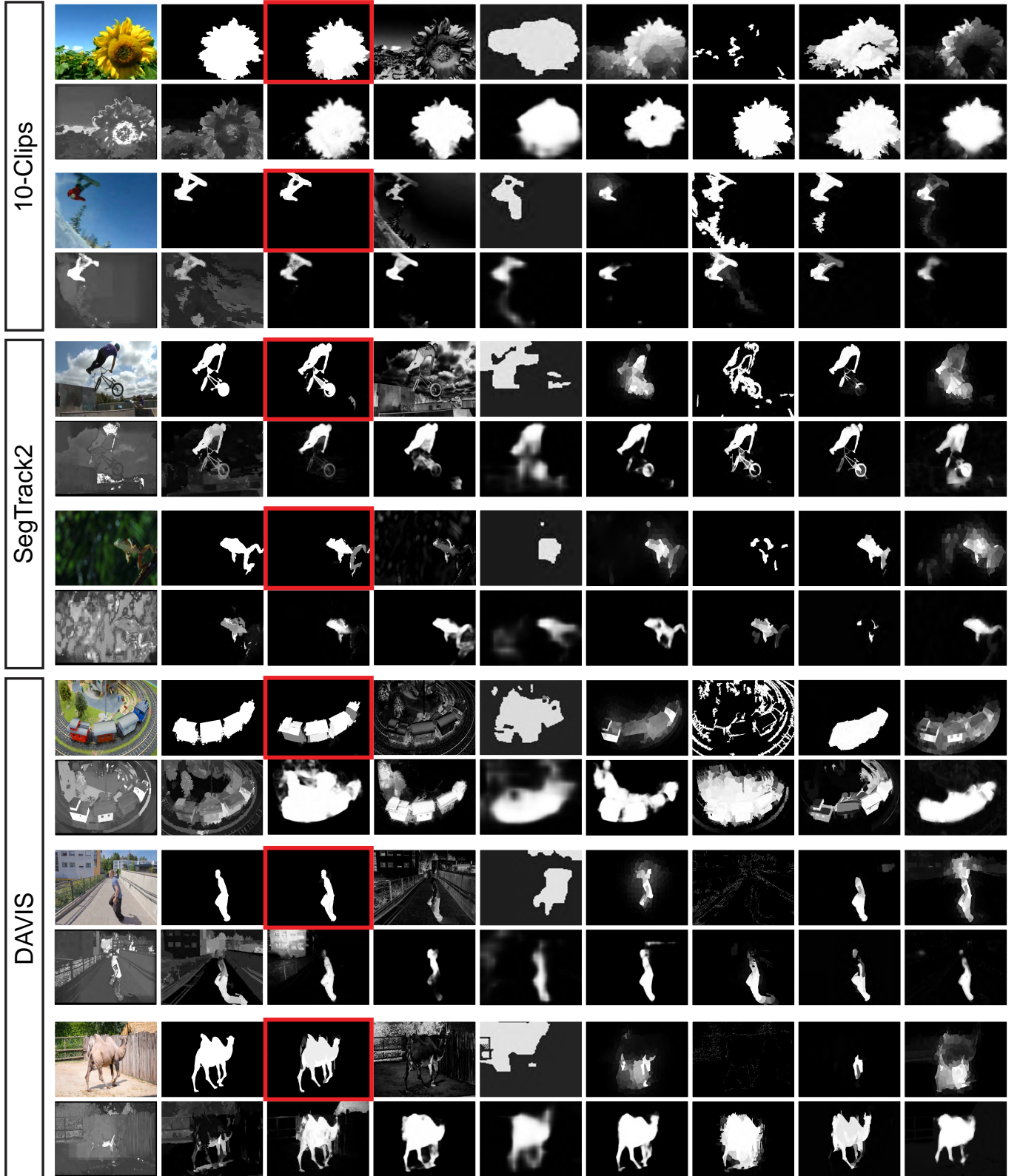


Fig. 5: Visual comparison of our method against the state-of-the-art methods. From top-left to bottom-right, original video frame and ground-truth are followed by outputs obtained using our method (STCRF), LC[20], LD[10], LGFOGR[21], LRSD[23], RST[6], SAG[22], SEG[19], STS[7], DCL[14], DHS[15], DS[26], DSS[17], ELD[16], MDF[24], and RFCN[25], in this order. Our method surrounded with red rectangles achieves the best results.

In order to quantitatively evaluate the obtained results, we first computed PRC and F-measure curves, which are shown in Figs. 6 and 7.

It can be seen that our method achieves the highest precision in almost the entire recall ranges on all the datasets. Especially on the two most challenging datasets (i.e., SegTrack2 and DAVIS), the performance gains of our method against the other methods are more remarkable (results with higher recall values are less important because achieving higher recall values is easy). When compared with the second best method, i.e., DHS, we see that (1) both the methods have comparable results on 10-Clips dataset, that (2) our method is significantly better than DHS on SegTrack2 dataset, and that (3) on DAVIS dataset, the precision of our method is larger than that of DHS when recall values are small (higher binarization thresholds) while it is smaller for large recall values (lower binarization thresholds). Salient object segmentation at higher thresholds is more practical and effective than that at lower thresholds because with low thresholds, more pixels are segmented regardless of salient objects or background.

F-measure indicates that our method significantly outperforms other methods at every threshold on all the datasets. Since the 10-Clips dataset is easiest among the three datasets, any methods can achieve good results while the other two datasets are challenging, meaning that the effectiveness of methods becomes discriminative. Indeed, compared with the second best method (DHS), our method is comparable on the 10-Clips dataset and significantly better on the other datasets.

Table III illustrates the evaluations in terms of F-Adap, F-Max, and MAE. Our proposed method achieves the best performance under all metrics on all datasets. In particular, outperformance of our method even against the second best method (DHS) is significant on SegTrack2 and DAVIS datasets.

### B. Detailed Analysis of the Proposed Method

To demonstrate the effectiveness of utilizing local and global deep features, that of utilizing spatiotemporal information in computing the saliency map, and that of multi-level analysis, we performed experiments under controlled settings and compared results.

1) *Effectiveness of combination of local and global deep features:* To evaluate the effectiveness of combining local and global deep features, we compared results using the STD feature with those using local deep feature alone, which is illustrated in Table IV.

We see that the combination of local and global deep features brings more gains than using only the local deep feature. This can be understood as follows. The local deep feature exploits the meaning of an object in terms of saliency but only in the small context, while the global deep feature can model the large context in the whole video block. Thus, the STD feature is more powerful. We remark that we also present results using the RGB feature instead of the deep feature just to confirm the deep feature outperforms the RGB feature.

2) *Effectiveness of spatiotemporal potential in STRCF:* To demonstrate the effectiveness of utilizing spatiotemporal

information into the energy function in STRCF, we performed experiments under four different controlled settings. Since spatiotemporal information is considered in the binary term of the energy function, we changed the binary term: setting  $\theta_{bt} = 0$  to use spatial information alone (denoted by SP), setting  $\theta_{bs} = 0$  to use temporal information alone (denoted by TP), and setting  $\theta_{bt} = \theta_{bs} = 0$  to use the unary term alone (denoted by U). We compared the proposed (complete) method (denoted by STP) with these three baseline methods (cf. Table V).

Table V indicates that STP exhibits the best performance on all metrics on the three datasets. We see that using both spatial and temporal information effectively works and brings more gains than that using spatial information alone or using temporal information alone. This suggests that our method captures spatial contexts on the frame and temporal information over frames to produce saliency maps.

3) *Effectiveness of multiple scale level approach:* In our method, we segment an input video at multiple scales. To demonstrate the effectiveness of this multiple scale approach, we compared methods that use different numbers of scale levels in computing the saliency map. More precisely, starting with only the coarsest scale level (level 1), we fused finer levels (levels 2, 3, 4) one by one to compute the saliency map. The methods are denoted by 1-level, 2-levels, 3-levels, and 4-levels (our complete method).

The results are illustrated in Table VI. Table VI shows that the multiple scale approach outperforms the single scale approach. It also indicates that using more scales produces better results. Indeed, as the number of scales in the saliency computation increases, we have more accurate results. Therefore, utilizing information from multiple scale levels empowers our method to gain benefit.

4) *Effective length for temporal segments:* We investigated the effectiveness of the size of the temporal segment to feed to STRCF by changing the window size from 1 to 64 by twice: 1, 2, 2<sup>2</sup>, ..., 2<sup>6</sup>. (cf. Table VII).

Table VII shows that as the window size become larger, we have more accurate results while the improvement in accuracy is saturated around the size of 16. On the other hand, the processing time for a larger window size is slow because the size of the graphical model becomes large. To balance the performance in accuracy and the processing time, we consider that the optimal window size of the temporal segment in this work is 16.

## VI. APPLICATION TO VIDEO OBJECT SEGMENTATION

Video object segmentation (VOS) is a binary labeling problem aiming to separate foreground objects from the background of a video[48]. On the other hand, salient object detection (SOD) aims to detect and segment salient objects in natural scenes. Although VOS and SOD are different tasks, SOD methods are beneficial for VOS when salient objects are main objects in scenes. In this section, we demonstrate the applicability of our proposed method to VOS.

Figure 8 illustrates the framework for VOS using the saliency map. In one pass, the output saliency map is binarized



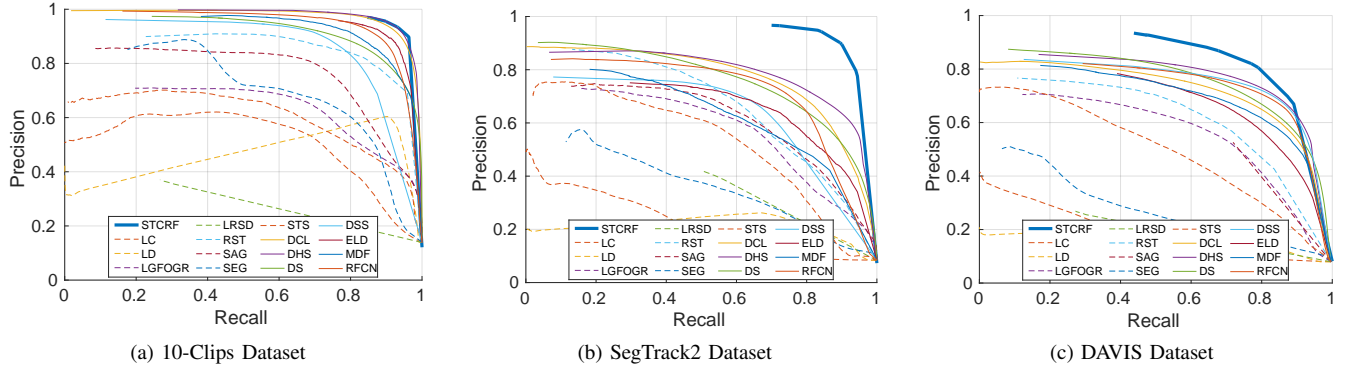


Fig. 6: Quantitative comparison of precision-recall curve with state-of-the-art methods under different thresholds. Our method is denoted by STCRF (thick blue).

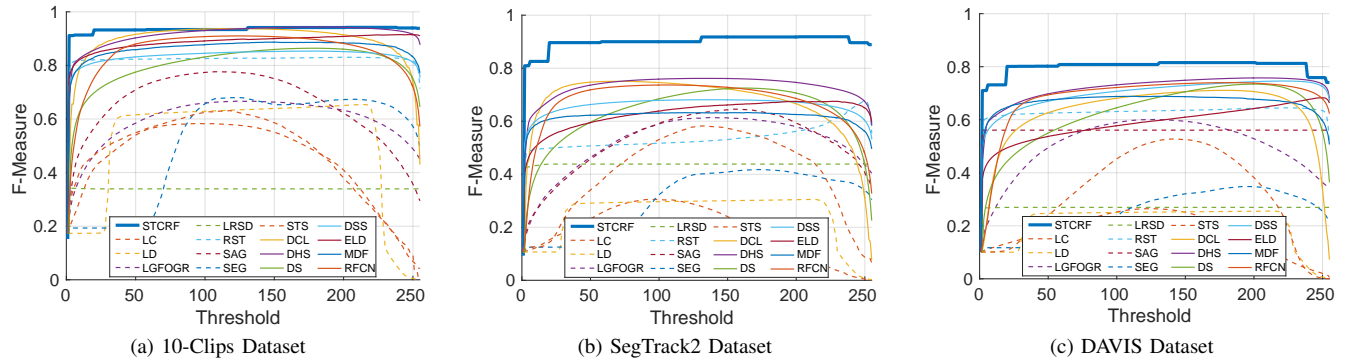


Fig. 7: Quantitative comparison of F-measure with state-of-the-art methods under different thresholds. Our method is denoted by STCRF (thick blue).

using the adaptive threshold mentioned in Section IV-B to obtain the foreground mask. In the other pass, we implemented the object segmentation method based on boundary snapping[54]. We first detect contours of foreground objects using CEDN, the method proposed by Yang et al.[55], and then apply the combinatorial grouping method[56] to compute the Ultrametric Contour Map (UCM) [56], which presents hierarchical segmentation. Superpixels are aligned by binarizing the UCM using threshold  $\tau = 0.3$ . From the foreground mask and superpixels, we perform majority voting to segment the foreground objects.

VOS methods are classified into two groups: one that is requiring the initial object mask at the first frame, and the other that is not. The former is called unsupervised while the latter is semi-supervised in the DAVIS Benchmark[48]. Since an initial object mask becomes a strong prior for accurately segmenting objects in subsequent frames, we chose most recent unsupervised methods for the fair comparison. We compared our method with the state-of-the-art saliency method (DHS[15]), and most recent unsupervised VOS methods: ACO[57], CVOS[58], FST[37], KEY[59], MSG[60], and NLC[61], and TRC[62]. We remark that for two SOD methods (our method and DHS), object segmentation is obtained using the framework in Fig. 8. We denote them by STCRF\* and DHS\*.

We tested all methods on the DAVIS dataset[48], the newest dataset for VOS, and evaluated results using measures in the 2017 DAVIS Challenge[63] (i.e., region similarity  $\mathcal{J}$ , contour accuracy  $\mathcal{F}$ , and overall performance  $\mathcal{O}$ ). For a given error measure, we consider three different statistics as done in [48]. They are the mean error, the object recall (measuring the fraction of sequences scoring higher than a threshold  $\tau = 0.5$ ), and the decay (quantifying the performance loss (or gain) over time). Note that the results of the compared state-of-the-art VOS techniques are used in the DAVIS Benchmark[48]<sup>2</sup>. We also note that we run the source code of ACO[57], which is not mentioned in the DAVIS Benchmark, provided by the authors with the recommended parameter settings. We set object masks using saliency methods including our proposed method and DHS[15] (denoted by DHS\*), as in Fig.8.

Figure 9 shows some examples of the obtained results. The quantitative comparison of these methods is shown in Table VIII, indicating that our proposed method STCRF\* exhibits the best performance on all metrics at all statistics. STCRF\* achieves 0.714 for  $\mathcal{J}(\text{Mean})$ , 0.674 for  $\mathcal{F}(\text{Mean})$ , and 0.694 for  $\mathcal{O}(\text{Mean})$ , while the best VOS method (NLC[61]) achieves 0.641, 0.593, and 0.617, respectively. STCRF\* outperforms the compared VOS methods by a large margin on all the metrics. We may thus conclude that our proposed SOD method works

<sup>2</sup>[http://davischallenge.org/soa\\_compare.html](http://davischallenge.org/soa_compare.html)

TABLE III: Quantitative comparison with state-of-the-art methods, using F-measure (F-Adap and F-Max) (higher is better) and Mean Absolute Errors (MAE) (smaller is better). The best and the second best results are shown in **blue** and **green**, respectively. Our method (STCRF) marked in **bold** is followed by methods for videos and those for still images.

Dataset Metric	10-Clips			SegTrack2			DAVIS		
	F-Adap $\uparrow$	F-Max $\uparrow$	MAE $\downarrow$	F-Adap $\uparrow$	F-Max $\uparrow$	MAE $\downarrow$	F-Adap $\uparrow$	F-Max $\uparrow$	MAE $\downarrow$
<b>STCRF</b>	<b>0.936</b>	<b>0.942</b>	<b>0.016</b>	<b>0.899</b>	<b>0.919</b>	<b>0.014</b>	<b>0.803</b>	<b>0.816</b>	<b>0.033</b>
LC[20]	0.577	0.583	0.166	0.244	0.306	0.173	0.201	0.265	0.191
LD[10]	0.637	0.654	0.197	0.286	0.305	0.281	0.252	0.256	0.302
LGFOGR[21]	0.629	0.667	0.207	0.500	0.614	0.117	0.537	0.601	0.102
LRSD[23]	0.339	0.342	0.164	0.438	0.438	0.102	0.269	0.269	0.116
RST[6]	0.827	0.831	0.055	0.510	0.677	0.125	0.627	0.645	0.077
SAG[22]	0.755	0.777	0.117	0.504	0.646	0.106	0.494	0.548	0.103
SEG[19]	0.687	0.680	0.298	0.388	0.418	0.321	0.305	0.348	0.323
STS[7]	0.591	0.631	0.177	0.471	0.583	0.147	0.379	0.527	0.183
DCL[14]	<b>0.935</b>	0.937	0.031	<b>0.734</b>	0.750	0.060	0.664	0.711	0.067
DHS[15]	0.923	<b>0.947</b>	<b>0.022</b>	0.733	<b>0.762</b>	<b>0.050</b>	<b>0.715</b>	<b>0.758</b>	<b>0.048</b>
DS[26]	0.832	0.864	0.050	0.636	0.725	0.069	0.616	0.734	0.076
DSS[17]	0.838	0.853	0.049	0.662	0.681	0.054	0.690	0.746	0.049
ELD[16]	0.893	0.915	0.023	0.611	0.675	0.065	0.572	0.683	0.081
MDF[24]	0.884	0.887	0.041	0.627	0.633	0.077	0.684	0.688	0.063
RFCN[25]	0.901	0.910	0.046	0.716	0.737	0.062	0.710	0.740	0.067

TABLE IV: Comparison of STD features and local deep features. The best results are shown in **blue** (higher is better for F-Adap and F-Max, and lower is better for MAE).

Used feature	10-Clips			SegTrack2			DAVIS		
	F-Adap $\uparrow$	F-Max $\uparrow$	MAE $\downarrow$	F-Adap $\uparrow$	F-Max $\uparrow$	MAE $\downarrow$	F-Adap $\uparrow$	F-Max $\uparrow$	MAE $\downarrow$
<b>STD feature</b>	<b>0.936</b>	<b>0.942</b>	<b>0.016</b>	<b>0.899</b>	<b>0.919</b>	<b>0.014</b>	<b>0.803</b>	<b>0.816</b>	<b>0.033</b>
Local feature alone	0.683	0.727	0.079	0.692	0.780	0.043	0.648	0.744	0.067
RGB feature	0.882	0.913	0.044	0.366	0.454	0.080	0.160	0.186	0.199

TABLE V: Comparison of different potentials in STCRF. The best results are shown in **blue** (higher is better for F-Adap and F-Max, and lower is better for MAE). Our complete method are marked in **bold**.

Setting description	Unary term	Spatial information	Temporal information	10-Clips			SegTrack2			DAVIS		
				F-Adap $\uparrow$	F-Max $\uparrow$	MAE $\downarrow$	F-Adap $\uparrow$	F-Max $\uparrow$	MAE $\downarrow$	F-Adap $\uparrow$	F-Max $\uparrow$	MAE $\downarrow$
STP	$\checkmark$	$\checkmark$	$\checkmark$	<b>0.936</b>	<b>0.942</b>	<b>0.016</b>	<b>0.899</b>	<b>0.919</b>	<b>0.014</b>	<b>0.803</b>	<b>0.816</b>	<b>0.033</b>
SP	$\checkmark$	$\times$	$\checkmark$	0.930	0.941	0.018	0.871	0.918	0.017	0.759	0.814	0.038
TP	$\checkmark$	$\checkmark$	$\times$	0.930	0.940	0.019	0.859	0.901	0.019	0.750	0.805	0.039
U	$\checkmark$	$\times$	$\times$	0.876	0.940	0.044	0.703	0.912	0.072	0.537	0.804	0.169

TABLE VI: Comparison of different numbers of scale levels in processing. The best results are shown in **blue** (higher is better for F-Adap and F-Max, and lower is better for MAE). Our complete method is marked in **bold**.

Setting description	10-Clips			SegTrack2			DAVIS		
	F-Adap $\uparrow$	F-Max $\uparrow$	MAE $\downarrow$	F-Adap $\uparrow$	F-Max $\uparrow$	MAE $\downarrow$	F-Adap $\uparrow$	F-Max $\uparrow$	MAE $\downarrow$
1-level	0.928	0.930	0.017	0.880	0.889	0.016	0.750	0.757	0.038
2-levels	0.929	0.940	0.017	0.876	0.908	0.015	0.763	0.800	0.035
3-levels	0.935	0.941	<b>0.016</b>	<b>0.909</b>	0.912	<b>0.014</b>	0.798	<b>0.816</b>	<b>0.033</b>
<b>4-levels</b>	<b>0.936</b>	<b>0.942</b>	<b>0.016</b>	0.899	<b>0.919</b>	<b>0.014</b>	<b>0.803</b>	<b>0.816</b>	<b>0.033</b>

even for VOS with satisfactory performance. We note that DHS\*, which is for SOD, is second best.

## VII. CONCLUSION

Differently from the still image, the video has temporal information and how to incorporate temporal information as effectively as possible is the essential issue for dealing with the video. This paper focused on detecting salient objects from a video and proposed a framework using STD features together with STCRF. Our method takes into account temporal information in a video as much as possible in different ways, namely, feature extraction and the saliency computation. Our proposed STD feature utilizes local and global contexts in both spatial and temporal domains. The proposed STD feature

based STCRF is capable of capturing temporal consistency of regions over frames and spatial relationship between regions.

Our experiments show that our proposed method significantly and consistently outperforms state-of-the-art methods on publicly available datasets. We also applied our saliency model to the video object segmentation task, experimentally showing that our method outperforms existing unsupervised methods on the DAVIS dataset.

## ACKNOWLEDGMENT

This work is in part supported by JST CREST (Grant No. JPMJCR14D1) and by Grant-in-Aid for Scientific Research (Grant No. 16H02851) of the Ministry of Education, Culture, Sports, Science and Technology of Japan.

TABLE VII: Comparison under different lengths of the temporal segment.

Length of temporal segment	10-Clips		SegTrack2		DAVIS	
	F-Adap $\uparrow$	MAE $\downarrow$	F-Adap $\uparrow$	MAE $\downarrow$	F-Adap $\uparrow$	MAE $\downarrow$
1 ( $= 2^0$ )	0.934	0.017	0.890	0.016	0.791	0.035
2 ( $= 2^1$ )	0.935	0.017	0.892	0.015	0.792	0.034
4 ( $= 2^2$ )	0.935	0.017	0.895	0.015	0.794	0.034
8 ( $= 2^3$ )	0.936	0.017	0.897	0.015	0.799	0.033
16 ( $= 2^4$ )	<b>0.936</b>	<b>0.016</b>	<b>0.899</b>	<b>0.014</b>	<b>0.803</b>	<b>0.033</b>
32 ( $= 2^5$ )	0.936	0.016	0.899	0.014	0.803	0.032
64 ( $= 2^6$ )	0.936	0.016	0.899	0.014	0.803	0.032

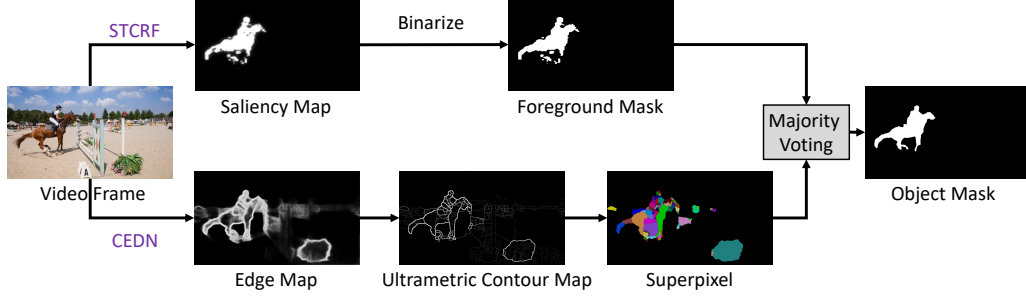


Fig. 8: Boundary snapping[54] based video object segmentation framework using the saliency map.

TABLE VIII: Quantitative comparison with state-of-the-art video object segmentation methods on the DAVIS dataset, using region similarity, contour accuracy, and overall performance metrics. The best three results are shown in blue, green, and red, respectively. Our method, denoted by STCRF\*, is marked in bold.

Methods	Region similarity ( $\mathcal{J}$ )			Contour accuracy ( $\mathcal{F}$ )			Overall performance ( $\mathcal{O}$ )
	Mean $\uparrow$	Recall $\uparrow$	Decay $\downarrow$	Mean $\uparrow$	Recall $\uparrow$	Decay $\downarrow$	Mean $\uparrow$
STCRF*	<b>0.714</b>	<b>0.851</b>	<b>-0.019</b>	<b>0.674</b>	<b>0.790</b>	<b>-0.019</b>	<b>0.694</b>
DHS*[15]	<b>0.701</b>	<b>0.840</b>	0.032	<b>0.656</b>	<b>0.779</b>	<b>0.036</b>	<b>0.679</b>
ACO[57]	0.503	0.572	<b>-0.006</b>	0.467	0.494	<b>-0.022</b>	0.592
CVOS[58]	0.514	0.581	0.127	0.490	0.578	0.138	0.502
FST[37]	0.575	0.652	0.044	0.536	0.579	0.065	0.556
KEY[59]	0.569	0.671	0.075	0.503	0.534	0.079	0.536
MSG[60]	0.543	0.636	<b>0.028</b>	0.525	0.613	0.057	0.534
NLC[61]	<b>0.641</b>	<b>0.731</b>	0.086	<b>0.593</b>	<b>0.658</b>	0.086	<b>0.617</b>
TRC[62]	0.501	0.560	0.050	0.478	0.519	0.066	0.490

## REFERENCES

- [1] T. Lu, Z. Yuan, Y. Huang, D. Wu, and H. Yu, "Video retargeting with nonlinear spatial-temporal saliency fusion," in *Image Processing (ICIP), 2010 17th IEEE International Conference on*, Sept 2010, pp. 1801–1804.
- [2] M. Guo, Y. Zhao, C. Zhang, and Z. Chen, "Fast object detection based on selective visual attention," *Neurocomput.*, vol. 144, pp. 184–197, Nov. 2014.
- [3] R. Zhao, W. Ouyang, and X. Wang, "Unsupervised saliency learning for person re-identification," in *Computer Vision and Pattern Recognition (CVPR), 2013 IEEE Conference on*, June 2013, pp. 3586–3593.
- [4] S. Stalder, H. Grabner, and L. Van Gool, "Dynamic objectness for adaptive tracking," in *Proceedings of the 11th Asian Conference on Computer Vision - Volume Part III*. Berlin, Heidelberg: Springer-Verlag, 2013, pp. 43–56.
- [5] W. Zhu, S. Liang, Y. Wei, and J. Sun, "Saliency optimization from robust background detection," in *Proceedings of the 2014 IEEE Conference on Computer Vision and Pattern Recognition*. Washington, DC, USA: IEEE Computer Society, 2014, pp. 2814–2821.
- [6] T.-N. Le and A. Sugimoto, "Contrast based hierarchical spatial-temporal saliency for video," in *Image and Video Technology - 7th Pacific-Rim Symposium, PSIVT 2015, Auckland, New Zealand, November 25-27, 2015, Revised Selected Papers*, ser. Lecture Notes in Computer Science, vol. 9431. Springer International Publishing Switzerland, 2015, pp. 734–748.
- [7] F. Zhou, S. B. Kang, and M. Cohen, "Time-mapping using space-time saliency," in *Computer Vision and Pattern Recognition (CVPR), 2014 IEEE Conference on*, June 2014, pp. 3358–3365.
- [8] L. Mai, Y. Niu, and F. Liu, "Saliency aggregation: A data-driven approach," in *Computer Vision and Pattern Recognition (CVPR), 2013 IEEE Conference on*, June 2013, pp. 1131–1138.
- [9] H. Jiang, J. Wang, Z. Yuan, Y. Wu, N. Zheng, and S. Li, "Salient object detection: A discriminative regional feature integration approach," in *Computer Vision and Pattern Recognition (CVPR), 2013 IEEE Conference on*, June 2013, pp. 2083–2090.
- [10] T. Liu, Z. Yuan, J. Sun, J. Wang, N. Zheng, X. Tang, and H.-Y. Shum, "Learning to detect a salient object," *Pattern Analysis and Machine Intelligence, IEEE Transactions on*, vol. 33, no. 2, pp. 353–367, Feb 2011.
- [11] P. Jiang, H. Ling, J. Yu, and J. Peng, "Salient region detection by ufo: Uniqueness, focusness and objectness," in *2013 IEEE International Conference on Computer Vision*, Dec 2013, pp. 1976–1983.
- [12] R. Girshick, J. Donahue, T. Darrell, and J. Malik, "Rich feature hierarchies for accurate object detection and semantic segmentation," in *2014 IEEE Conference on Computer Vision and Pattern Recognition*, June 2014, pp. 580–587.
- [13] D. Tran, L. Bourdev, R. Fergus, L. Torresani, and M. Paluri, "Learning spatiotemporal features with 3D convolutional networks," in *2015 IEEE International Conference on Computer Vision (ICCV)*, Dec 2015, pp. 4489–4497.
- [14] G. Li and Y. Yu, "Deep contrast learning for salient object detection," in *2016 IEEE Conference on Computer Vision and Pattern Recognition (CVPR)*, June 2016, pp. 478–487.
- [15] N. Liu and J. Han, "Dhsnet: Deep hierarchical saliency network for salient object detection," in *2016 IEEE Conference on Computer Vision and Pattern Recognition (CVPR)*, June 2016, pp. 678–686.
- [16] G. Lee, Y. W. Tai, and J. Kim, "Deep saliency with encoded low level

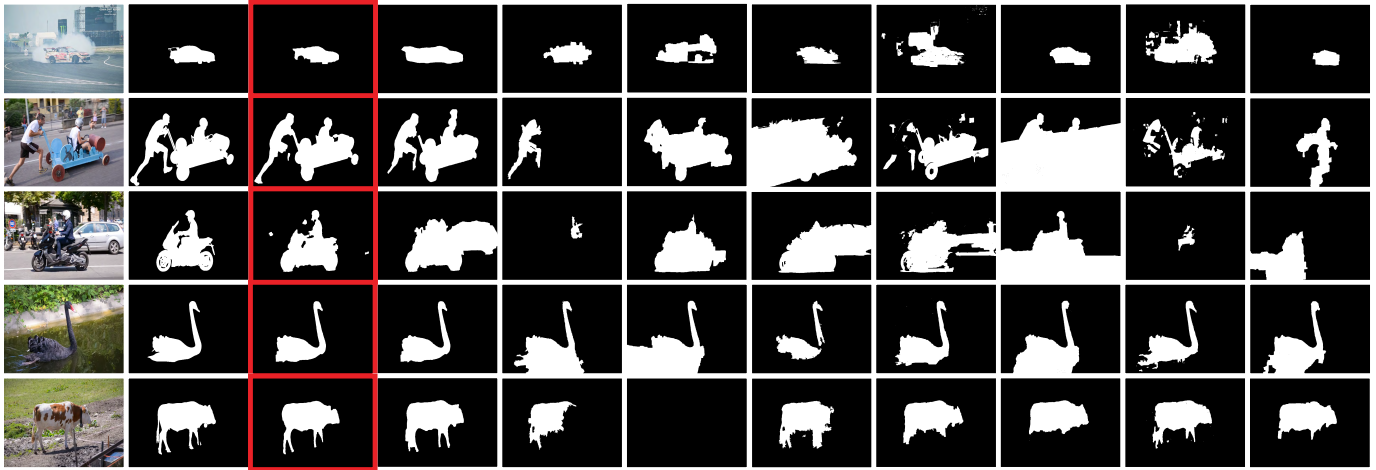


Fig. 9: Visual comparison of our method against the state-of-the-art video object segmentation methods. From left to right, original video frame and ground-truth are followed by outputs obtained using our method (STCRF\*), DHS\*[15], ACO[57], CVOS[58], FST[37], KEY[59], MSG[60], NLC[61], and TRC[62], in this order. Our STCRF surrounded with red rectangles achieves the best results.

- distance map and high level features,” in *2016 IEEE Conference on Computer Vision and Pattern Recognition (CVPR)*, June 2016, pp. 660–668.
- [17] Q. Hou, M.-M. Cheng, X. Hu, A. Borji, Z. Tu, and P. Torr, “Deeply supervised salient object detection with short connections,” in *Proceedings of the IEEE Conference on Computer Vision and Pattern Recognition*, 2017.
- [18] T.-N. Le and A. Sugimoto, “Spatiotemporal utilization of feep features for video saliency detection,” in *Proceedings of the ICME Workshop on Deep Learning for Intelligent Multimedia Analytics (DeLIMMA)*, 2017.
- [19] E. Rahtu, J. Kannala, M. Salo, and J. Heikkilä, “Segmenting salient objects from images and videos,” in *Computer Vision - ECCV 2010 - 11th European Conference on Computer Vision, Heraklion, Crete, Greece, September 5-11, 2010, Proceedings, Part V*. Springer, 2010, pp. 366–379.
- [20] Y. Zhai and M. Shah, “Visual attention detection in video sequences using spatiotemporal cues,” in *Proceedings of the 14th ACM International Conference on Multimedia*, ACM. New York, NY, USA: ACM, 2006, pp. 815–824.
- [21] W. Wang, J. Shen, and L. Shao, “Consistent video saliency using local gradient flow optimization and global refinement,” *Image Processing, IEEE Transactions on*, vol. 24, no. 11, pp. 4185–4196, Nov 2015.
- [22] W. Wang, J. Shen, and F. Porikli, “Saliency-aware geodesic video object segmentation,” in *Computer Vision and Pattern Recognition (CVPR), 2015 IEEE Conference on*, June 2015, pp. 3395–3402.
- [23] Y. Xue, X. Guo, and X. Cao, “Motion saliency detection using low-rank and sparse decomposition,” in *2012 IEEE International Conference on Acoustics, Speech and Signal Processing (ICASSP)*, March 2012, pp. 1485–1488.
- [24] G. Li and Y. Yu, “Visual saliency based on multiscale deep features,” in *Computer Vision and Pattern Recognition (CVPR), 2015 IEEE Conference on*, June 2015, pp. 5455–5463.
- [25] L. Wang, L. Wang, H. Lu, P. Zhang, and X. Ruan, *Saliency Detection with Recurrent Fully Convolutional Networks*. Springer International Publishing, 2016, pp. 825–841.
- [26] X. Li, L. Zhao, L. Wei, M.-H. Yang, F. Wu, Y. Zhuang, H. Ling, and J. Wang, “Deepsaliency: Multi-task deep neural network model for salient object detection,” *IEEE Transactions on Image Processing*, vol. 25, no. 8, pp. 3919–3930, Aug 2016.
- [27] W. Shimoda and K. Yanai, “Distinct class-specific saliency maps for weakly supervised semantic segmentation,” in *Computer Vision - ECCV 2016: 14th European Conference, Amsterdam, The Netherlands, October 11-14, 2016, Proceedings, Part IV*. Springer International Publishing, 2016, pp. 218–234.
- [28] P. Krähenbühl and V. Koltun, “Efficient inference in fully connected CRFs with gaussian edge potentials,” in *Advances in Neural Information Processing Systems 24*, J. Shawe-Taylor, R. S. Zemel, P. L. Bartlett, F. Pereira, and K. Q. Weinberger, Eds. Curran Associates, Inc., 2011, pp. 109–117.
- [29] Y. Wang and Q. Ji, “A dynamic conditional random field model for object segmentation in image sequences,” in *2005 IEEE Computer Society Conference on Computer Vision and Pattern Recognition (CVPR’05)*, vol. 1, June 2005, pp. 264–270.
- [30] Y. Wang, K.-F. Loe, and J.-K. Wu, “A dynamic conditional random field model for foreground and shadow segmentation,” *IEEE Transactions on Pattern Analysis and Machine Intelligence*, vol. 28, no. 2, pp. 279–289, Feb 2006.
- [31] R. Yi, J. Wang, and P. Tan, “Automatic fence segmentation in videos of dynamic scenes,” in *The IEEE Conference on Computer Vision and Pattern Recognition (CVPR)*, June 2016.
- [32] C. P. Yu, H. Le, G. Zelinsky, and D. Samaras, “Efficient video segmentation using parametric graph partitioning,” in *2015 IEEE International Conference on Computer Vision (ICCV)*, Dec 2015, pp. 3155–3163.
- [33] O. Russakovsky, J. Deng, H. Su, J. Krause, S. Satheesh, S. Ma, Z. Huang, A. Karpathy, A. Khosla, M. Bernstein, A. C. Berg, and L. Fei-Fei, “ImageNet Large Scale Visual Recognition Challenge,” *International Journal of Computer Vision (IJCV)*, vol. 115, no. 3, pp. 211–252, 2015.
- [34] A. Karpathy, G. Toderici, S. Shetty, T. Leung, R. Sukthankar, and L. Fei-Fei, “Large-scale video classification with convolutional neural networks,” in *Proceedings of the 2014 IEEE Conference on Computer Vision and Pattern Recognition*. Washington, DC, USA: IEEE Computer Society, 2014, pp. 1725–1732.
- [35] L. Wang, H. Lu, X. Ruan, and M.-H. Yang, “Deep networks for saliency detection via local estimation and global search,” in *Computer Vision and Pattern Recognition (CVPR), 2015 IEEE Conference on*, June 2015, pp. 3183–3192.
- [36] V. Nair and G. E. Hinton, “Rectified linear units improve restricted boltzmann machines,” in *Proceedings of the 27th International Conference on Machine Learning (ICML-10)*, J. Frnkranz and T. Joachims, Eds. Omnipress, 2010, pp. 807–814.
- [37] A. Papazoglou and V. Ferrari, “Fast object segmentation in unconstrained video,” in *Computer Vision (ICCV), 2013 IEEE International Conference on*. IEEE, Dec 2013, pp. 1777–1784.
- [38] C. Rother, V. Kolmogorov, and A. Blake, “grabcut”: Interactive foreground extraction using iterated graph cuts,” *ACM Trans. Graph.*, vol. 23, no. 3, pp. 309–314, Aug. 2004.
- [39] P. Weinzaepfel, J. Revaud, Z. Harchaoui, and C. Schmid, “Deepflow: Large displacement optical flow with deep matching,” in *2013 IEEE International Conference on Computer Vision*, Dec 2013, pp. 1385–1392.
- [40] M. M. Cheng, V. A. Prisacariu, S. Zheng, P. H. S. Torr, and C. Rother, “Densecut: Densely connected crfs for realtime grabcut,” *Comput. Graph. Forum*, vol. 34, no. 7, pp. 193–201, Oct. 2015.

- [41] T.-N. Le, K.-T. Nguyen, M.-H. Nguyen-Phan, T.-V. Ton, T.-A. N. (2), X.-S. Trinh, Q.-H. Dinh, V.-T. Nguyen, A.-D. Duong, A. Sugimoto, T. V. Nguyen, and M.-T. Tran, "Instance re-identification flow for video object segmentation," *The 2017 DAVIS Challenge on Video Object Segmentation - CVPR Workshops*, 2017.
- [42] Y. H. Tsai, M. H. Yang, and M. J. Black, "Video segmentation via object flow," in *2016 IEEE Conference on Computer Vision and Pattern Recognition (CVPR)*, June 2016, pp. 3899–3908.
- [43] T. K. Moon, "The expectation-maximization algorithm," *IEEE Signal processing magazine*, vol. 13, no. 6, pp. 47–60, 1996.
- [44] Y. Boykov, O. Veksler, and R. Zabih, "Fast approximate energy minimization via graph cuts," *Pattern Analysis and Machine Intelligence, IEEE Transactions on*, vol. 23, no. 11, pp. 1222–1239, Nov 2001.
- [45] L. R. Foulds, *Graph theory applications*. Springer Science & Business Media, 2012.
- [46] K. Fukuchi, K. Miyazato, A. Kimura, S. Takagi, and J. Yamato, "Saliency-based video segmentation with graph cuts and sequentially updated priors," in *Multimedia and Expo, 2009. ICME 2009. IEEE International Conference on*. IEEE, June 2009, pp. 638–641.
- [47] F. Li, T. Kim, A. Humayun, D. Tsai, and J. M. Rehg, "Video segmentation by tracking many figure-ground segments," in *2013 IEEE International Conference on Computer Vision*, Dec 2013, pp. 2192–2199.
- [48] F. Perazzi, J. Pont-Tuset, B. McWilliams, L. V. Gool, M. Gross, and A. Sorkine-Hornung, "A benchmark dataset and evaluation methodology for video object segmentation," in *2016 IEEE Conference on Computer Vision and Pattern Recognition (CVPR)*, June 2016, pp. 724–732.
- [49] R. Achanta, S. Hemami, F. Estrada, and S. Susstrunk, "Frequency-tuned salient region detection," in *Computer Vision and Pattern Recognition, 2009. CVPR 2009. IEEE Conference on*. IEEE, June 2009, pp. 1597–1604.
- [50] Y. Jia and M. Han, "Category-independent object-level saliency detection," in *Computer Vision (ICCV), 2013 IEEE International Conference on*. IEEE, Dec 2013, pp. 1761–1768.
- [51] A. Borji, M. M. Cheng, H. Jiang, and J. Li, "Salient object detection: A benchmark," *IEEE Transactions on Image Processing*, vol. 24, no. 12, pp. 5706–5722, Dec 2015.
- [52] Y. Jia, E. Shelhamer, J. Donahue, S. Karayev, J. Long, R. Girshick, S. Guadarrama, and T. Darrell, "Caffe: Convolutional architecture for fast feature embedding," in *Proceedings of the 22Nd ACM International Conference on Multimedia*, ser. MM '14. New York, NY, USA: ACM, 2014, pp. 675–678.
- [53] D. E. Rumelhart, G. E. Hinton, and R. J. Williams, "Learning representations by back-propagating errors," in *Neurocomputing: Foundations of Research*. Cambridge, MA, USA: MIT Press, 1988, pp. 696–699.
- [54] S. Caelles, K.-K. Maninis, J. Pont-Tuset, L. Leal-Taixé, D. Cremers, and L. Van Gool, "One-shot video object segmentation," in *Computer Vision and Pattern Recognition (CVPR)*, 2017.
- [55] J. Yang, B. Price, S. Cohen, H. Lee, and M. H. Yang, "Object contour detection with a fully convolutional encoder-decoder network," in *2016 IEEE Conference on Computer Vision and Pattern Recognition (CVPR)*, June 2016, pp. 193–202.
- [56] J. Pont-Tuset, P. Arbelaz, J. T. Barron, F. Marques, and J. Malik, "Multiscale combinatorial grouping for image segmentation and object proposal generation," *IEEE Transactions on Pattern Analysis and Machine Intelligence*, vol. 39, no. 1, pp. 128–140, Jan 2017.
- [57] W. D. Jang, C. Lee, and C. S. Kim, "Primary object segmentation in videos via alternate convex optimization of foreground and background distributions," in *2016 IEEE Conference on Computer Vision and Pattern Recognition (CVPR)*, June 2016, pp. 696–704.
- [58] B. Taylor, V. Karasev, and S. Soatto, "Causal video object segmentation from persistence of occlusions," in *2015 IEEE Conference on Computer Vision and Pattern Recognition (CVPR)*, June 2015, pp. 4268–4276.
- [59] Y. J. Lee, J. Kim, and K. Grauman, "Key-segments for video object segmentation," in *2011 International Conference on Computer Vision*, Nov 2011, pp. 1995–2002.
- [60] P. Ochs and T. Brox, "Object segmentation in video: A hierarchical variational approach for turning point trajectories into dense regions," in *2011 International Conference on Computer Vision*, Nov 2011, pp. 1583–1590.
- [61] A. Faktor and M. Irani, "Video segmentation by non-local consensus voting," *The British Machine Vision Conference(BMVC)*, vol. 2, no. 7, p. 8, 2014.
- [62] K. Fragkiadaki, G. Zhang, and J. Shi, "Video segmentation by tracing discontinuities in a trajectory embedding," in *2012 IEEE Conference on Computer Vision and Pattern Recognition*, June 2012, pp. 1846–1853.
- [63] J. Pont-Tuset, F. Perazzi, S. Caelles, P. Arbeláez, A. Sorkine-Hornung, and L. Van Gool, "The 2017 davis challenge on video object segmentation," *arXiv:1704.00675*, 2017.